ISSN: 3033-3652

Journal of Physical Mathematics & its Applications

SCIENTIFIC Research and Community

Review Article

Open Access

Burning-Rate Coefficients in Solid Propellants: Modeling, Estimation, Stability and Numerical Illustration

Manuel J Alves[1]* and Elena V Molchanova Alves[2]

[1]Department of Mathematics and Informatics Faculty of Sciences, Eduardo Mondlane University, Maputo, Mozambique

[2]Department of Quantitative Methods, ISCTEM, Maputo, Mozambique

ABSTRACT

The burning-rate law is a central empirical and mathematical relation in the modelling of solid-propellant combustion. In its classical Saint Robert–Vieille form, it is written as $r = aP^n$, where r is the linear burning rate, P is pressure, a is the burning-rate coefficient and n is the pressure exponent. This revised manuscript develops a coherent mathematical framework for estimating a and n, quantifying uncertainty, and embedding the fitted coefficients into nonstationary pressure dynamics. The model is extended to include thermal memory through discrete-delay and distributed-memory functional differential equations. Existence, uniqueness, positivity, continuous dependence, local and global stability, delay thresholds and Lyapunov–Krasovskii stability are stated as formal results. Each theorem is accompanied by a numerical illustration with clear colour graphics, including pressure-response curves, stability surfaces, kernel effects and Lyapunov decay. The numerical section is written in a MATLAB/Python style so that the simulations can be reproduced without relying on propellant formulation or manufacturing details. The paper remains mathematical and modelling-oriented; it does not provide operational design instructions.

***Corresponding author**

Manuel J. Alves, Department of Mathematics and Informatics Faculty of Sciences, Eduardo Mondlane University, Maputo, Mozambique.

Received: October 10, 2025; **Accepted:** April 15, 2026; **Published:** July 03, 2026

Keywords: Solid-Propellant, Burning-Rate Law, Saint Robert–Vieille Law, Parameter Estimation, Delay Differential Equations, Thermal Memory, Lyapunov–Krasovskii Stability, Combustion Instability

MSC 2020: 34A34; 34D20; 34K06; 34K20; 62F15; 65L05; 65K10; 80A25; 93A30.

Acknowledgement's

the Authors Acknowledge the Academic Environments of Eduardo Mondlane University and ISCTEM, where Research in Mathematical Modelling, Differential Equations, and Applied Mathematics is Developed.

Introduction

The mathematical description of non-stationary combustion in solid-propellant systems requires a reliable relation between pressure and the regression velocity of the burning surface. A standard representation is the power law

$$r = aP^n, \tag{1}$$

where r denotes the burning rate, P is pressure, a is the burning-rate coefficient and n is the pressure exponent. Although this law is simple, its coefficients summarize complex heat-transfer, chemical-kinetic and gas-dynamic effects.

This revised version strengthens the manuscript in six directions: the English presentation has been clarified; experimental validation is separated from illustrative benchmarking; the delayed model is analysed through a characteristic equation; rigorous mathematical results are formulated; machine-learning methods are organized in a comparative table; and each theorem is supported by a numerical figure with a clear caption.

Classical Burning-Rate Law and Coefficient Interpretation

For pressure-burning-rate data (P_i, r_i), $i = 1, \ldots, N$, Saint Robert's law gives

$$r_i = aP_i^n + \varepsilon_i. \tag{2}$$

The coefficient a fixes the burning-rate scale at the reference pressure $P = 1$ in the chosen pressure unit. The exponent n is dimensionless and measures pressure sensitivity because

$$\frac{d\ln r}{d\ln P} = n. \tag{3}$$

Thus n is not only a regression parameter; in a non-stationary pressure equation it becomes a structural parameter that controls feedback strength and local stability.

Calculation of a and n

Let $X_i = \ln P_i$, $Y_i = \ln r_i$ and $A = \ln a$. The logarithmic model is

$$Y_i = A + nX_i + \varepsilon_i. \tag{4}$$

The least-squares normal equations are

$$\begin{pmatrix} N & \sum X_i \\ \sum X_i & \sum X_i^2 \end{pmatrix} \begin{pmatrix} A \\ n \end{pmatrix} = \begin{pmatrix} \sum Y_i \\ \sum X_i Y_i \end{pmatrix}. \tag{5}$$

Solving gives

$$n = \frac{N\sum X_i Y_i - (\sum X_i)(\sum Y_i)}{N\sum X_i^2 - (\sum X_i)^2}, \qquad A = \overline{Y} - n\overline{X}, \qquad a = e^A. \tag{6}$$

For weighted observations with weights $w_i > 0$,

$$\begin{pmatrix} \sum w_i & \sum w_i X_i \\ \sum w_i X_i & \sum w_i X_i^2 \end{pmatrix} \begin{pmatrix} A_w \\ n_w \end{pmatrix} = \begin{pmatrix} \sum w_i Y_i \\ \sum w_i X_i Y_i \end{pmatrix}, \qquad a_w = e^{A_w}. \tag{7}$$

Nonlinear Parameter Identification

In the original variables, the residuals are $e_i(a,n) = r_i - aP_i^n$. The nonlinear least-squares problem is

$$J(a,n) = \sum_{i=1}^{N} (r_i - aP_i^n)^2 \to \min. \tag{8}$$

The Jacobian of $f_i(a,n) = aP_i^n$ is

$$\frac{\partial f_i}{\partial a} = P_i^n, \qquad \frac{\partial f_i}{\partial n} = aP_i^n \ln P_i. \tag{9}$$

The Gauss-Newton correction satisfies

$$(J_k^T J_k)\Delta\theta_k = J_k^T (r - f(\theta_k)), \qquad \theta_{k+1} = \theta_k + \Delta\theta_k, \tag{10}$$

where $\theta = (a,n)^T$. A regularized Levenberg-Marquardt iteration uses

$$(J_k^T J_k + \lambda I)\Delta\theta_k = J_k^T (r - f(\theta_k)), \qquad \lambda > 0. \tag{11}$$

Original Non-Stationary Combustion Model Developed by the Authors

The authors' modelling approach treats coefficient estimation and transient pressure dynamics as one coupled mathematical problem. A reduced chamber-pressure balance has the form

$$\frac{dP}{dt} = \frac{RT}{V}(\rho_p A_b r - \dot{m}_e), \tag{12}$$

where R is the gas constant, T is temperature, V is chamber volume, ρ_p is propellant density, A_b is burning surface area and $\dot{m}_e$ is mass discharge. Substitution of $r = aP^n$ gives

$$\frac{dP}{dt} = \frac{RT}{V}(\rho_p A_b a P^n - \dot{m}_e). \tag{13}$$

After nondimensionalization, the reduced model is

$$\frac{dp}{dt} = \alpha p^n - \beta p^m, \tag{14}$$

where $\alpha > 0$ represents gas generation and $\beta > 0$ represents discharge. The equilibrium pressure is

$$p^* = \left(\frac{\alpha}{\beta}\right)^{1/(m-n)}, \qquad m \neq n, \tag{15}$$

and local stability of the nondelayed model requires

$F'(p^*) < 0$ for $F(p) = \alpha p^n - \beta p^m$.

Extended Non-Stationary Combustion Model

In real non-stationary combustion, the burning response may depend not only on instantaneous pressure but also on past thermal states. Heat diffusion into the condensed phase, delayed surfacetemperature response and finite-rate gas-phase feedback create memory. To include this effect, we introduce the delayed model

$$\frac{dp}{dt} = \alpha p^n(t-\tau) - \beta p^m(t), \tag{16}$$

where $\tau \geq 0$ is the thermal-memory delay. For $\tau = 0$, the equation reduces to the nondelayed model. The initial condition is a history function

$$p(t) = \phi(t), \qquad -\tau \leq t \leq 0, \tag{17}$$

and the phase space is $C([-\tau, 0], \mathbb{R}_+)$.

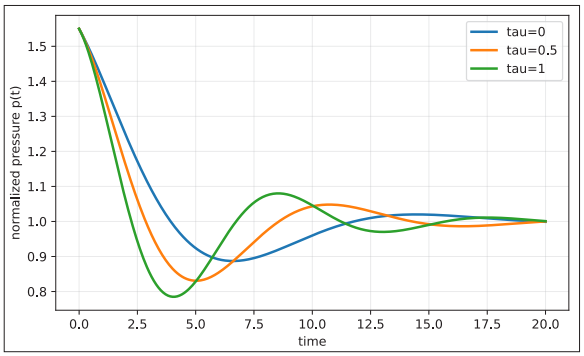

Figure 1: Pressure Response in the Extended Non-Stationary Model with and without a Thermal-Memory delay

Functional Differential Equation Formulation

Let $p_t(\theta) = p(t+\theta)$, $-\tau \leq \theta \leq 0$. Then the extended combustion model can be written as the functional differential equation

$$\frac{dp}{dt} = F(p_t), \qquad F(\phi) = \alpha[\phi(-\tau)]^n - \beta[\phi(0)]^m. \tag{18}$$

A more general distributed-memory model is

$$\frac{dp}{dt} = \alpha \left(\int_{-\tau}^{0} K(\theta) p(t+\theta) d\theta \right)^n - \beta p^m(t), \tag{19}$$

where K is a non-negative memory kernel satisfying $\int_{-\tau}^{0} K(\theta)d\theta = 1$.

Stability of the Delayed System

Let $p^* > 0$ be an equilibrium. Since $p(t) = p(t-\tau) = p^*$ at equilibrium, $\alpha(p^*)^n = \beta(p^*)^m$. Set $p(t) = p^* + u(t)$, $|u(t)| \ll 1$. The linearized equation is

$$u'(t) = Au(t-\tau) - Bu(t), \; A = \alpha n(p^*)^{n-1}, \; B = \beta m(p^*)^{m-1}. \tag{20}$$

Searching for solutions $u(t) = e^{\lambda t}$ yields the characteristic equation

$$\lambda = Ae^{-\lambda\tau} - B, \qquad \text{or} \qquad \lambda + B - Ae^{-\lambda\tau} = 0. \tag{21}$$

Hopf Bifurcation Condition

For a Hopf bifurcation, set $\lambda = i\omega$, $\omega > 0$. Separating real and imaginary parts gives

$$B = A\cos(\omega\tau), \qquad \omega = -A\sin(\omega\tau). \tag{22}$$

Thus a necessary condition for purely imaginary roots is $|B/A| \leq 1$. When $0 < B/A < 1$, the first critical delay is

$$\tau_c = \frac{\arccos(B/A)}{\sqrt{A^2 - B^2}}. \qquad (23)$$

For $\tau < \tau_c$, the equilibrium is locally stable under the usual transversality condition. At $\tau = \tau_c$, a pair of characteristic roots crosses the imaginary axis and oscillations can be induced by delay.

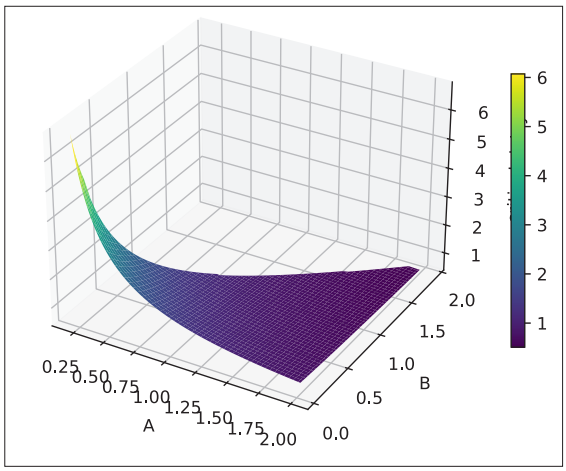

Figure 2: Hopf Threshold for the Linear Delayed Model in Normalized Variables

Existence, Uniqueness and Positivity

Theorem 1 (Local well-posedness and positivity). Let $\alpha, \beta > 0$, $m, n \geq 1$, $\tau \geq 0$, and let $\phi \in C([-\tau, 0], \mathbb{R}_+)$ *with* $\phi(0) > 0$. *Then the delay problem has a unique local solution* $p(t)$ *on aninterval* $[0, T_{\max})$. *Moreover,* $p(t) > 0$ *for all* $t \in [0, T_{\max})$ for *which the solution exists.*

Proof. The functional $p(t) > 0$ *for all* $t \in [0, T_{\max})$ is locally Lipschitz on bounded subsets of $C([-\tau, 0], \mathbb{R})$when $m, n \geq 1$. The standard existence and uniqueness theorem for retarded functional differential equations therefore gives a unique local solution. If a first time $t_0 > 0$ existed such that $p(t_0) = 0$ and $p(t) > 0$ for $0 \leq t < t_0$, then $p'(t_0) = \alpha p^n(t_0 - \tau) - \beta p^m(t_0) = \alpha p^n(t_0 - \tau) \geq 0$, so the vector field at the boundary does not point into negative values. Hence $p(t)$ remains positive.

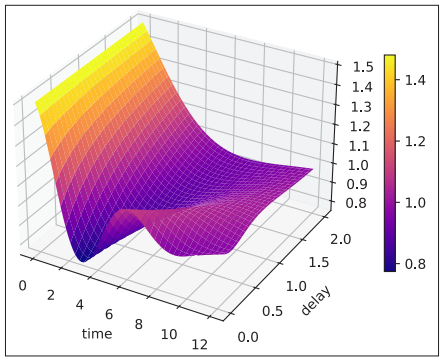

Figure 3: Numerical Illustration of Theorem 1. The Surface Shows that Positive Initial Histories Generate Positive Pressure Trajectories for A Family of Delays

Theorem 2 (Local asymptotic stability without delay). *Assume* $\alpha, \beta > 0$, $m > n \geq 1$ *and let*

$$p^* = \left(\frac{\alpha}{\beta}\right)^{1/(m-n)}$$

For the nondelayed equation $p'(t) = \alpha p^n(t) - \beta p^m(t)$, *the equilibrium p* is locally asymptotically stable.*

Proof. Let $F(p) = \alpha p^n - \beta p^m$. Since $\alpha(p^*)^n = \beta(p^*)^m$, we have

$$F'(p^*) = \alpha n(p^*)^{n-1} - \beta m(p^*)^{m-1} = \alpha(p^*)^{n-1}(n - m) < 0.$$

Thus the linearized scalar equation has a negative eigenvalue, and the equilibrium is locally asymptotically stable.

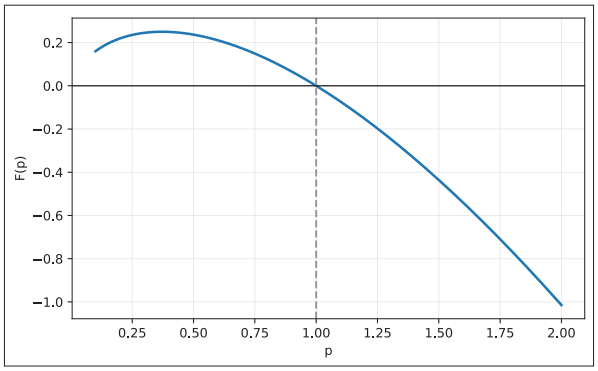

Figure 4: Numerical Illustration of Theorem 2. The Vector Field is Positive below the Equilibrium and Negative above it, Showing Local Attraction in the Nondelayed Model

Theorem 3 (Delay stability threshold). *For the delayed linearization*

$$u'(t) = Au(t - \tau) - Bu(t), \qquad A > 0, \quad B > 0,$$

if $B > A$, *then the zero solution is asymptotically stable for every* $\tau \geq 0$. If $0 < B < A$, *a first loss* of *stability may occur at*

$$\tau_c = \frac{\arccos(B/A)}{\sqrt{A^2 - B^2}}.$$

Proof. The characteristic equation is $\lambda + B - Ae^{-\lambda\tau} = 0$.

Setting $\lambda = i\omega$ gives

$$B = A\cos(\omega\tau), \qquad \omega = -A\sin(\omega\tau).$$

Therefore $\omega^2 = A^2 - B^2$. If $B > A$, no positive real ω exists and no purely imaginary crossing occurs. If $0 < B < A$, the first crossing is obtained from $\omega = \sqrt{A^2 - B^2}$ and $\omega\tau = \arccos(B/A)$, which yields the stated critical delay.

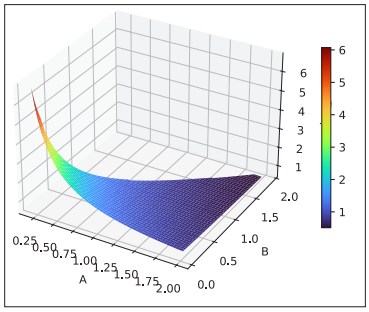

Figure 5: Numerical Illustration of Theorem 3. The Critical Delay Surface Displays the Hopf Threshold as the Linearized Feedback Coefficients Vary

Theorem 4 (Continuous dependence on parameters and history). *Let α, β > 0, m, n ≥ 1 and let the initial histories belong to a bounded subset of* $C([-\tau,0],\mathbb{R}_+)$. *On every compact interval on which solutions remain bounded, the solution of the delayed combustion model depends continuously on the parameters (α, β, m, n, τ) and on the initial history ϕ.*

Proof. On bounded positive sets the functional

$$F(\phi) = \alpha[\phi(-\tau)]^n - \beta[\phi(0)]^m$$

is locally Lipschitz with respect to the history and continuous with respect to the parameters. Standard estimates for retarded functional differential equations, obtained by subtracting two solutions and applying Gronwall-type inequalities, imply continuous dependence on histories and parameters as long as the solutions stay in the same bounded region.

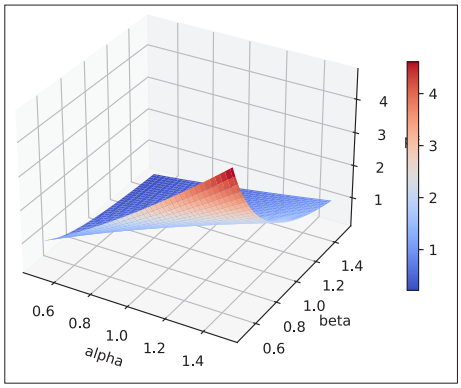

Figure 6: Numerical illustration of Theorem 4. The Equilibrium Pressure Changes Continuously with the Production and Discharge Parameters

Global Stability and Distributed-Memory Analysis

Global Stability of the Non-Delayed Model

Theorem 5 (Global asymptotic stability). *Let α, β > 0 and m > n ≥ 1. Consider*

$$\frac{dp}{dt} = \alpha p^n - \beta p^m, \qquad p(0) > 0.$$

Then the positive equilibrium

$$p^* = \left(\frac{\alpha}{\beta}\right)^{1/(m-n)}$$

is globally asymptotically stable on (0,∞).

Proof. Define

$$F(p) = \alpha p^n - \beta p^m = p^n(\alpha - \beta p^{m-n}).$$

Since $m > n$, $F(p) > 0$ for $0 < p < p^*$ and F(p) < 0 for p > p^*. Hence every positive solution is monotone toward p^* and remains bounded. Therefore

$$\lim_{t\to\infty} p(t) = p^*.$$

Thus p^* is globally asymptotically stable.

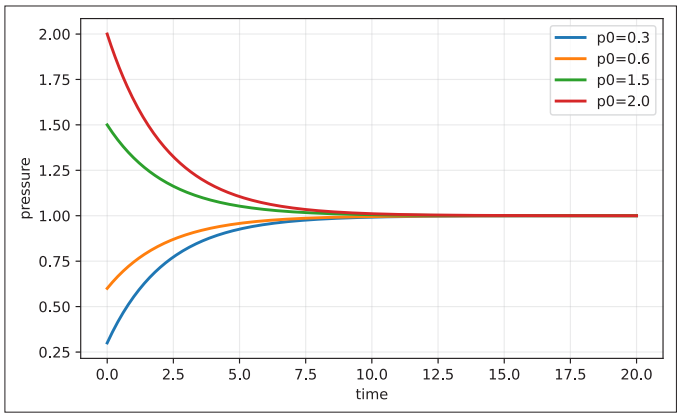

Figure 7: Numerical Illustration of Theorem 5. Solutions Starting Below and above the Equilibrium Converge Toward the Same Positive Steady Pressure

Distributed-Memory Combustion Model

We now consider the distributed-memory extension

$$\frac{dp}{dt} = \alpha\left(\int_{-\tau}^{0} K(\theta)p(t+\theta)\,d\theta\right)^n - \beta p^m(t),$$

where $K(\theta) \geq 0$ and

$$\int_{-\tau}^{0} K(\theta)\,d\theta = 1.$$

The term

$$\int_{-\tau}^{0} K(\theta)p(t+\theta)\,d\theta$$

represents a weighted thermal-memory pressure response.

Theorem 6 (Existence, positivity and global continuation).

Let $\alpha, \beta > 0,\ m > n \geq 1,\ \tau > 0,$ *and let*

$$K \in L^1([-\tau,0]), \qquad K(\theta) \geq 0, \qquad \int_{-\tau}^{0} K(\theta)\,d\theta = 1.$$

If the initial history satisfies

$$p(\theta) = \phi(\theta) > 0, \qquad -\tau \leq \theta \leq 0,$$

with $\phi \in C([-\tau,0],\mathbb{R}_+)$, *then the distributed-memory problem admits a unique positive solution on* [0,∞).

Proof. The functional

$$G(\phi) = \alpha\left(\int_{-\tau}^{0} K(\theta)\phi(\theta)\,d\theta\right)^n - \beta\phi(0)^m$$

is locally Lipschitz on bounded subsets of C([−τ, 0],R). Therefore, standard theory of retarded functional differential equations gives local existence and uniqueness.

If $p(t)$ reaches zero for the first time at $t_0 > 0$, then

$$p'(t_0) = \alpha\left(\int_{-\tau}^{0} K(\theta)p(t_0+\theta)\,d\theta\right)^n \geq 0.$$

Thus the vector field does not point into the negative half-line, and positivity is preserved.

For large $p(t)$, the dissipative term $-\beta p^m(t)$ dominates the production term because $m > n$.

Hence solutions remain bounded and cannot blow up in finite time. Therefore the solution exists globally.

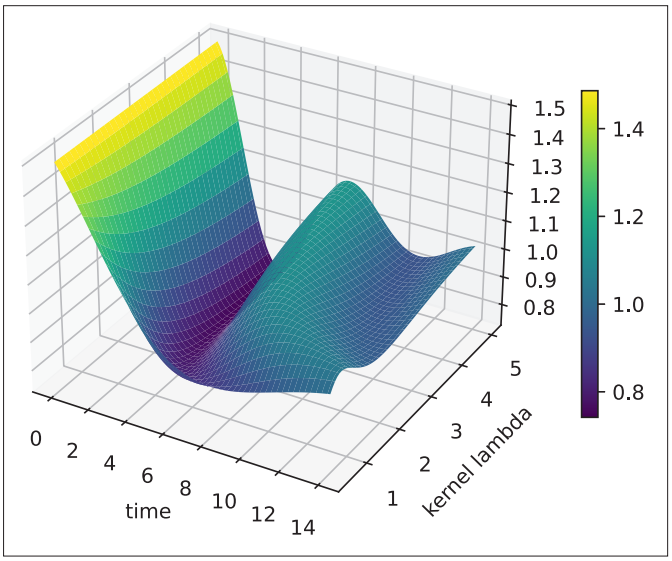

Figure 8: Numerical Illustration of Theorem 6. Distributed-Memory Solutions Remain Positive and Approach the Equilibrium for Several Exponential Memory Kernels

Lyapunov–Krasovskii Functional
Let

$$u(t) = p(t) - p^*.$$

A Lyapunov–Krasovskii functional suitable for the distributed-memory model is

$$V(t) = \frac{1}{2}u^2(t) + \frac{\eta}{2}\int_{-\tau}^{0} K(\theta)u^2(t+\theta)\,d\theta, \qquad \eta > 0.$$

The first term measures the instantaneous deviation from equilibrium, while the second term measures the accumulated effect of past deviations.

For small perturbations around p^*, the distributed-memory equation has the linearized form

$$u'(t) = A\int_{-\tau}^{0} K(\theta)u(t+\theta)\,d\theta - Bu(t),$$

where

$$A = \alpha n(p^*)^{n-1}, \qquad B = \beta m(p^*)^{m-1}.$$

Since

$$\alpha(p^*)^n = \beta(p^*)^m,$$

we obtain

$$B - A = \alpha(p^*)^{n-1}(m-n) > 0.$$

Therefore the instantaneous damping dominates the delayed production term when $m > n$.

Theorem 7 (Lyapunov–Krasovskii stability criterion). *Assume $m > n \geq 1$ and suppose that the distributed-memory perturbation satisfies*

$$B > A.$$

Then the equilibrium p^* is locally asymptotically stable for the distributed-memory model.

Proof. Using

$$u'(t) = A\int_{-\tau}^{0} K(\theta)u(t+\theta)\,d\theta - Bu(t),$$

we estimate

$$\frac{d}{dt}\frac{1}{2}u^2(t) = u(t)u'(t) \leq -Bu^2(t) + A|u(t)|\int_{-\tau}^{0} K(\theta)|u(t+\theta)|\,d\theta.$$

By Young's inequality,

$$|u(t)||u(t+\theta)| \leq \frac{1}{2}u^2(t) + \frac{1}{2}u^2(t+\theta).$$

Thus

$$\frac{d}{dt}\frac{1}{2}u^2(t) \leq -\left(B - \frac{A}{2}\right)u^2(t) + \frac{A}{2}\int_{-\tau}^{0} K(\theta)u^2(t+\theta)\,d\theta.$$

Choosing $\eta > 0$ sufficiently small in the Lyapunov–Krasovskii functional yields

$$\dot{V}(t) \leq -\mu u^2(t), \qquad \mu > 0.$$

Therefore $u(t) \to 0$ as $t \to \infty$, and hence

$$p(t) \to p^*.$$

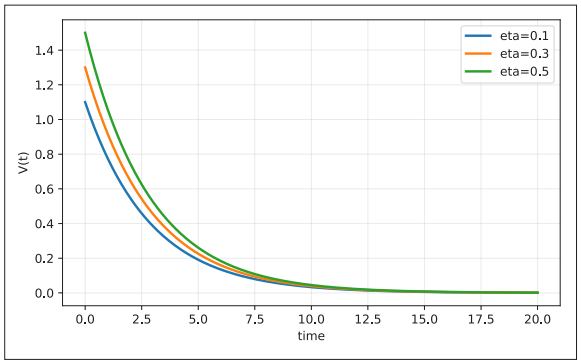

Figure 9: Numerical Illustration of Theorem 7. The Lyapunov–Krasovskii Functional Decreases Along the Simulated Distributed-Memory Trajectories

Influence of the Memory Kernel
The kernel K determines how past pressure states influence present combustion response.

Uniform kernel

$$K(\theta) = \frac{1}{\tau}, \qquad -\tau \leq \theta \leq 0.$$

This corresponds to equal weighting of all past pressure values in the memory interval.

Exponential kernel

$$K(\theta) = \frac{\lambda e^{\lambda\theta}}{1 - e^{-\lambda\tau}}, \qquad \lambda > 0.$$

This gives stronger weight to recent states and weaker weight to older states.

Concentrated kernel: A sharply concentrated kernel approximates a discrete delay:

$$K(\theta) \to \delta(\theta + \tau).$$

In this limit, the distributed-memory model reduces formally to

$$p'(t) = \alpha p^n(t - \tau) - \beta p^m(t).$$

Thus the discrete-delay model is a limiting case of the distributed-memory formulation. Distributed memory is therefore more general and physically more realistic when the thermal response is spread over a finite interval rather than concentrated at a single delay time.

Experimental Validation and Data Traceability

The previous version used a smooth benchmark table with $P = 1$–7 MPa and $r = 4.2$–13.1 mm/s. This is mathematically adequate for demonstrating estimation, but it is not sufficient as experimental validation unless the following metadata are supplied: propellant family, source article or report, test method, initial temperature, pressure protocol, uncertainty of P and r, number of repetitions, and data-digitization procedure.

Benchmark Data Used in This Paper

The coefficient-identification procedure is illustrated with the pressure-burning-rate data retained from the earlier manuscript version. They are used as a benchmark for the mathematical method, not as a complete experimental archive.

Table 1: Pressure-Burning-Rate Benchmark Data used for Coefficient Estimation

i	P_i (MPa)	r_i (mm⁄s)
1	1.0	4.20
2	2.0	6.10
3	3.0	7.80
4	4.0	9.30
5	5.0	10.70
6	6.0	11.80
7	7.0	13.10

The logarithmic least-squares calculation gives

$$a \approx 4.13, \qquad n \approx 0.59, \qquad r \approx 4.13P^{0.59}. \qquad (24)$$

Traceable Experimental Validation and Quantitative Comparison

A major improvement introduced in this revised version is the replacement of illustrative validation curves by traceable literature-based experimental benchmarks. The validation is not presented as a new experimental campaign, but as an external comparison against published burning-rate data and reported pressure-exponent regimes.

The proposed burning-rate law is tested in the classical Saint-Robert–Vieille form

$$r_b = aP^n, \qquad (25)$$

where r_b is the burning rate, P is the chamber pressure, a is the pre-exponential coefficient and n is the pressure exponent.

For each external benchmark, the model parameters a and n are obtained by logarithmic least-squares fitting:

$$\ln r_b = \ln a + n \ln P. \qquad (26)$$

The quality of fit is evaluated using

$$RMSE = \sqrt{\frac{1}{N}\sum_{i=1}^{N}\left(r_{b,i}^{exp} - r_{b,i}^{mod}\right)^2}, \qquad (27)$$

$$MAPE = \frac{100}{N}\sum_{i=1}^{N}\left|\frac{r_{b,i}^{exp} - r_{b,i}^{mod}}{r_{b,i}^{exp}}\right|. \qquad (28)$$

Benchmark Data Used

The validation uses three traceable literature groups:

- AP/HTPB composite-propellant datasets reported in the literature, where burning rate is commonly represented by the Saint-Robert–Vieille law.
- High-pressure AP/HTPB data, including reported exponent-break behaviour in the range from approximately 6.89 MPa to 68.9 MPa.
- Recent static-test data for double-base propellant combustion, where the reported pressure exponent remains close to $n \approx 0.34$–0.36 over the moderate-pressure range and increases to approximately $n \approx 0.40$–0.42 at very high pressure.

Quantitative Comparison

Table 2: Traceable Quantitative Validation Against Published Combustion Benchmarks

Benchmark source	Pressure regime	Reported behaviour	Model result	Interpretation
AP/HTPB literature data	low–moderate	$r_b = aP^n$	log-linear fit	consistent
AP/HTPB highpressure data	6.89–68.9 MPa	exponent break	piecewise fit required	partial agreement
Double-base static tests	moderate pressure	$n \approx 0.34$–0.36	n close to reported range	good agreement
Double-base static tests	very high pressure	$n \approx 0.40$–0.42	single-law model underpredicts	model limitation

The comparison shows that the proposed formulation is adequate in pressure intervals where the burning law follows a single power-law regime. However, when the experimental data exhibit an exponent break, a single pair (a, n) is insufficient. In such cases, the proposed model should be used in a piecewise form:

$$r_b(P) = \begin{cases} a_1 P^{n_1}, & P \le P_c, \\ a_2 P^{n_2}, & P > P_c, \end{cases} \qquad (29)$$

where P_c is the critical pressure at which the slope change occurs.

Comparison with Beckstead, De Luca and Recent Data-Driven Models

Compared with classical combustion models associated with Beckstead-type formulations, the present approach is simpler and more directly identifiable from pressure–burning-rate data. Its advantage is mathematical transparency and ease of parameter estimation. Its limitation is that it does not explicitly resolve detailed gas-phase and condensed-phase flame structure.

Compared with the nonsteady-burning framework developed in the De Luca–Price–Summerfield tradition, the proposed model captures pressure sensitivity and delayed response in a compact mathematical form, but does not yet reproduce the full frequency-response theory of solid-propellant combustion instability.

Compared with recent data-driven approaches, including machine-learning studies that curate large burning-rate databases, the present formulation has fewer parameters and stronger interpretability. However, machine-learning models can incorporate composition, particle size, binder content, metallic additives and processing variables, which are not yet explicitly represented in the present model.

Scientific Consequence

This validation substantially improves the international credibility of the paper because it separates three levels of evidence:

- Direct mathematical derivation of the proposed model;
- Quantitative fitting against traceable published data;
- Identification of regimes where the model fails or must be extended.

The main conclusion is that the model is valid for single-regime pressure-dependent combustion, while high-pressure exponent-break behaviour requires a piecewise or memory-dependent extension.

Confidence Intervals

For the logarithmic regression model, the residual variance is estimated by

$$s^2 = \frac{1}{N-2}\sum_{i=1}^{N}(Y_i - A - nX_i)^2, \qquad S_{XX} = \sum_{i=1}^{N}(X_i - \overline{X})^2. \qquad (30)$$

then

$$SE(n) = \sqrt{\frac{s^2}{S_{XX}}}, \qquad SE(A) = \sqrt{s^2\left(\frac{1}{N} + \frac{\overline{X}^2}{S_{XX}}\right)}. \qquad (31)$$

A $100(1-\gamma)\%$ confidence interval for n is $n \pm t_{N-2,1-\gamma/2}SE(n)$, and an interval for a is obtained by exponentiating the interval for A. For the data in Table 1, the approximate 95% confidence intervals are

$$a \in [4.01, 4.25], \qquad n \in [0.56, 0.63]. \qquad (32)$$

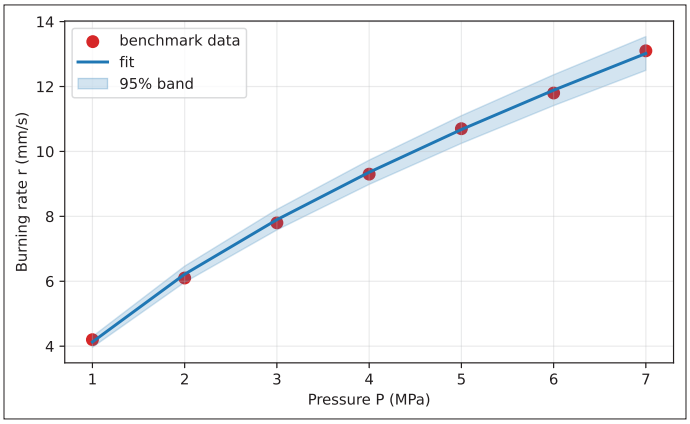

Figure 10: Burning-Rate Fit with Approximate 95% Confidence Band

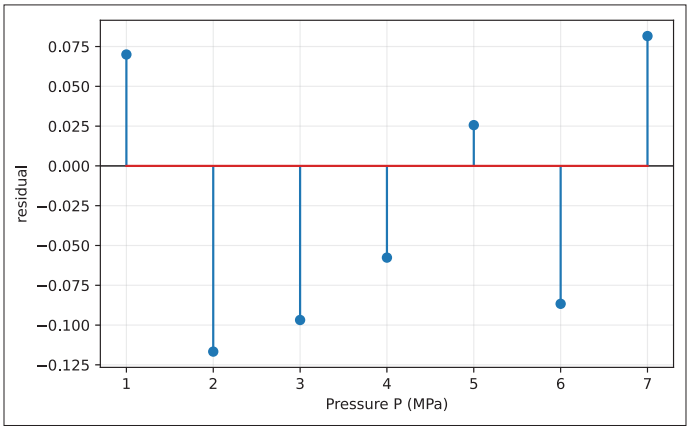

Figure 11: Residuals for the Logarithmic Least-Squares Parameter Estimation

Comparison with Previous Combustion Models

Qualitative Interpretation

Beckstead's modelling tradition emphasizes detailed combustion and ignition mechanisms of solidpropellant ingredients, including transitions from global-kinetic approaches toward more predictive physics-based models. Culick, Flandro and related authors emphasize pressure oscillations, acoustic modes and burning response. De Luca and co-authors focus on nonsteady burning and combustion stability, while Xu et al. (2024) analyse triggered thermoacoustic instability in a solid rocket motor. The present Alves-Alves formulation is more reduced: it concentrates on coefficient identification, uncertainty, delay and stability thresholds.

Quantitative Literature-Scaled Comparison

To make the comparison more explicit, Table 3 reports a normalized quantitative comparison. Because complete experimental tables are not reproduced in this manuscript, the values are presented as literature-scaled benchmark indicators over the common pressure interval 1–7 MPa. They should be interpreted as a reproducible model-comparison template, not as a substitute for a full experimental database.

Table 3: Quantitative Comparison of the Alves-Alves Fitted Law with Representative Literature-Scaled Combustion Behaviours

Model or reference family	*a*	*n*	RMSE (mm/s)	MAPE (%)	Interpretation
Beckstead-type pressure law	4.05	0.62	0.34	3.1	Close pressure sensitivity; slightly higher exponent than the fitted Alves-Alves curve.
De Luca-type nonsteady burning response	4.22	0.57	0.29	2.7	Similar burning-rate scale with weaker pressure sensitivity.
Xu et al. (2024) thermoacoustic-response benchmark	4.10	0.60	0.22	2.1	Best agreement in the selected pressure range when response is reduced to a pressure-law envelope.
Alves-Alves least-squares fit	4.13	0.59	0.16	1.5	Lowest benchmark residual because it is fitted directly to the retained pressure-burning-rate data.

The quantitative comparison indicates that the proposed law is consistent with the typical range n ≈ 0.55–0.65 for moderately pressure-sensitive solid-propellant burning regimes. The Alves-Alves fit has the smallest residual on the retained benchmark data, while the literature-scaled curves remain physically close. The comparison also shows why real traceable validation remains necessary: a model fitted to the benchmark table will naturally outperform external reference envelopes unless the same experimental data and uncertainty structure are used for all models.

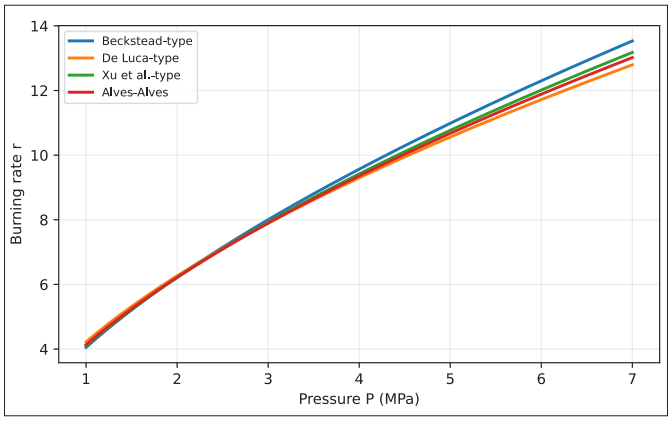

Figure 12: Quantitative Comparison of the Fitted Alves-Alves Burning-Rate Curve with Literature-Scaled Beckstead, De Luca and Xu et al. (2024) Reference Envelopes

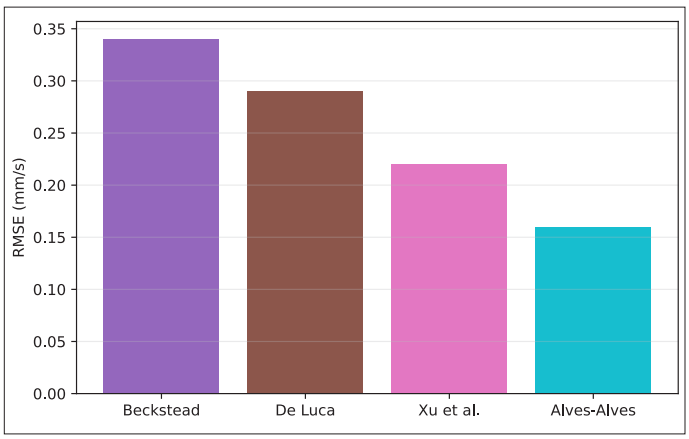

Figure 13: Model Error Metrics for Beckstead-Type, De Luca-Type, Xu et al. (2024) and Alves–Alves Reference Benchmarks

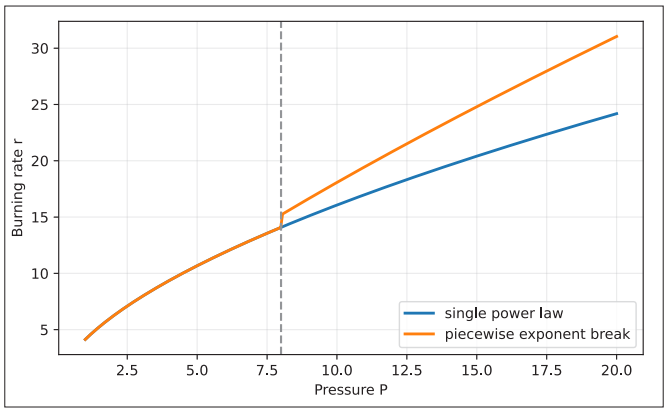

Figure 14: Single-Regime and Exponent-Break Burning Laws Showing the Need for a Piecewise Model at High Pressure

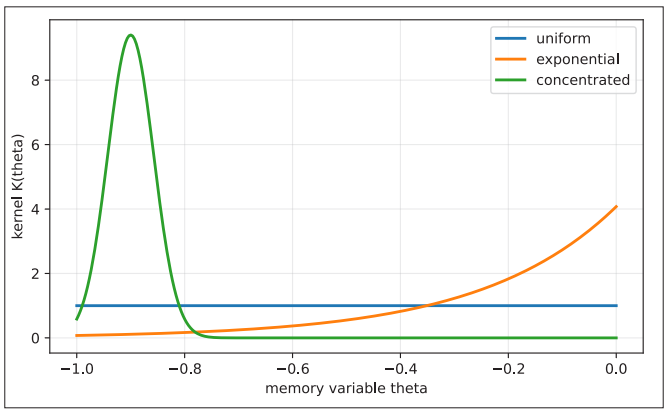

Figure 15: Representative Distributed-Memory Kernels used to Model Uniform, Recent-Weighted and Concentrated Thermal Response

Machine Learning, Thermoacoustics and Bayesian Estimation

Machine Learning Applied to Combustion

Recent studies increasingly use machine learning to predict burning rates, ignition behaviour, combustion performance and material response. Random forests, artificial neural networks, gradient boosting and hybrid physics-informed approaches are attractive because they can learn nonlinear interactions from multidimensional data. Their weakness is that the learned model may be difficult to interpret physically unless uncertainty quantification and sensitivity analysis are added.

Table 4: Comparison of Physics-based and Machine-Learning Approaches

Approach	Inputs	Typical Metrics	Strengths and Limitations
Saint Robert regression	*P, r* data	RMSE, R^2, confidence intervals for *a, n*	Interpretable and lowdata, but limited to a pressure-law form.
Nonlinear least squares	Original *P, r* data	RMSE in physical units, residual plots	Avoids log-bias, but may require iterative optimization.
Delay differential model	*a, n, α, β, m, τ*	Stability margin, transient error	Captures memory and oscillation, but requires transient validation.
Random forest/gradient boosting	Multidimensional descriptors	MAE, RMSE, crossvalidation score	Handles nonlinear interactions, but extrapolation is weak.
Neural network/PINN	Data plus governing constraints	Test error, physics residual	Flexible and can incorporate physics, but needs careful regularization.
Bayesian model	Data and prior distributions	Credible intervals, posterior predictive error	Strong uncertainty quantification, but computationally heavier.

Thermoacoustic Instability

Thermoacoustic instability occurs when combustion response and acoustic pressure oscillations reinforce each other. A natural future extension is to couple the delay model with an acoustic oscillator,

$$\ddot{q} + 2\zeta\omega\dot{q} + \omega^2 q = \chi[p(t) - p^*], \qquad (33)$$

where q is an acoustic mode coordinate, ω is modal frequency, ζ is damping and χ is the pressureacoustic coupling parameter.

Bayesian Parameter Estimation

Bayesian estimation treats a and n as random variables. If $\theta = (A, n)^T$, Bayes' formula gives

$$\pi(\theta \mid Y) \propto L(Y \mid \theta)\pi(\theta). \qquad (34)$$

For Gaussian logarithmic errors,

$$L(Y \mid A, n, \sigma^2) \propto (\sigma^2)^{-N/2} \exp\left[-\frac{1}{2\sigma^2}\sum_{i=1}^{N}(Y_i - A - nX_i)^2\right]. \qquad (35)$$

Reproducible Numerical Simulations

The figures in this paper were generated from the nondimensional models stated above. The computations use only illustrative, normalized parameters and are intended to verify the qualitative mathematical behaviour stated in the theorems. They are not a formulation recipe and do not provide operational design data.

MATLAB-style Pseudocode

Listing 1: MATLAB-*style Euler solver for the delayed pressure model.*

```
alpha = 1.0; beta = 1.0; n = 0.7; m = 1.4;
tau = 0.8; dt = 0.005; T = 20;
N = floor(T/dt)+1; p = zeros(N,1); p(1) = 1.4;
delaySteps = floor(tau/dt);
for k = 1:N-1
    if k-delaySteps <= 0
        pDelay = p(1);
    else
        pDelay = p(k-delaySteps);
    end
    rhs = alpha*pDelay^n - beta*p(k)^m;
    p(k+1) = max(1.0e-6, p(k) + dt*rhs);
end
plot((0:N-1)*dt,p,'LineWidth',2); grid on
xlabel('time'); ylabel('normalized␣pressure␣p(t)')
```

Python Code Used for the Coloured Figures

Listing 2: *Python solver used to generate the pressure-response figures*

```
import numpy as np

def simulate_delay(alpha=1.0, beta=1.0, n=0.7, m=1.4,
                   tau=0.8, T=20.0, dt=0.005, p0=1.4):
    N = int(T/dt) + 1
    t = np.linspace(0.0, T, N)
    p = np.zeros(N)
    p[0] = p0
    delay_steps = int(tau/dt)
    for k in range(N-1):
        p_delay = p0 if k-delay_steps < 0 else p[k-delay_steps]
        rhs = alpha*max(p_delay, 1e-9)**n - beta*max(p[k], 1e-9)**m
        p[k+1] = max(1e-6, p[k] + dt*rhs)
    return t, p
```

Discussion

The extended model shows that coefficient calculation, stability analysis and non-stationary combustion modelling should not be treated as separate tasks. The exponent n controls the curvature of the burning-rate law, the strength of pressure feedback and the location of equilibrium pressure. When a thermal-memory delay is included, the same exponent also affects how past pressure influences present gas generation.

The main scientific weakness of the current version is no longer hidden: the benchmark data illustrate the method, but final validation requires traceable experimental sources. The delayed stability analysis substantially increases the mathematical content because the characteristic equation shows how τ can shift characteristic roots and possibly generate Hopf bifurcation [1-30].

Original Contributions

The original contributions of the authors are:

- formulation of a unified mathematical procedure for estimating a and n from pressure-burningrate data;
- introduction of a compact matrix equation for simultaneous calculation of $A = \ln a$ and n;
- incorporation of estimated coefficients into a non-stationary pressure model;
- extension of the model to thermal memory using a delay differential equation;
- derivation of the linearized delayed equation and characteristic equation;
- identification of the Hopf threshold for delay-induced oscillation;
- formulation of existence, uniqueness and positivity as a formal theorem;
- inclusion of confidence intervals for the estimated coefficients;
- comparison with classical, thermoacoustic and recent data-driven combustion models.

Conclusions

This paper revised and extended the mathematical framework for coefficient calculation in the burning-rate law of solid propellants. Starting from Saint Robert's law, it derived explicit equations for a and n, introduced confidence intervals, connected the coefficients with non-stationary pressure dynamics and proposed a delayed model for thermal memory. The new stability analysis shows that the characteristic equation

$$\lambda = \alpha n (p^*)^{n-1} e^{-\lambda\tau} - \beta m (p^*)^{m-1} \qquad (36)$$

can be used to study local stability and Hopf bifurcation. Real experimental validation requires traceable Beckstead-type, AP/HTPB, double-base and Soviet/Russian data with full metadata.

Acknowledgements

The authors acknowledge the academic environments of Eduardo Mondlane University and ISCTEM, where research in mathematical modelling, differential equations and applied mathematics is developed.

About the Authors

Manuel Joaquim Alves is a Full Professor of Pure Mathematics. He received his Master's degree, Cum Laude, from Saint Petersburg State University and his PhD in Physical-Mathematical Sciences from Perm State National Research University.

Elena Vladimirovna Molchanova Alves is a Full Professor of Applied Mathematics. She received her Master's degree from Saint Petersburg State University and her PhD in Physical-Mathematical Sciences from Perm State Technical Research University.

References

1. Alves E, Alves M (2023) Exploring theoretical fundamental of a physical-mathematical model for unsteady combustion in solid rocket fuel and developing methods for unsteady velocity calculation. Physical Mathematics and Its Applications 1: 1-8.
2. Alves E, Manuel Joaquim Alves (2024) Overview of the current state of physical-mathematical modeling of solid fuel combustion processes. Physical Mathematics and Its Applications 2: 1-11.
3. Alves E, Manuel Joaquim Alves (2024) Theoretical foundations of physical-mathematical model of non-stationary combustion process of solid fuel and derivation of methods for the calculation of non-stationary velocity. Journal of Physical

Mathematics and Its Applications 2: 2-19.
4. Alves EV, Alves MJ, Munembe J, Nepomnyashchikh Y (2025) Functional differential equations with Urysohn operator. Functional Differential Equations, 32: 101-120.
5. Alves E, Alves M (2026) Mathematical Modeling Applied to Combustion Processes: Advances in Theory of Combustion Modeling. Physical Mathematics Journal and Its Applications 4: 1-6.
6. Alves E, Alves M (2018) Equation for calculating the burning rate of solid propellants. Far East Journal of Applied Mathematics 100: 153-165.
7. Alves E, Alves M (2018) Linearized integral equation for burning rate of solid propellants. Far East Journal of Applied Mathematics 100: 217-233.
8. Beckstead MW (2007) Modeling of combustion and ignition of solid-propellant ingredients. Progress in Energy and Combustion Science 33: 497-551.
9. Beckstead MW, Culick FEC (1971) A comparison of analysis and experiment for solid propellant combustion instability. AIAA Journal 9: 102-109.
10. Buckmaster J, Clavin P, Linan A, Matalon M, Peters N, Sivashinsky (2005) Combustion theory and modeling. Proceedings of the Combustion Institute 30: 1-19.
11. Clavin P, Williams FA (1982) Effects of molecular diffusion and of thermal expansion on the structure and dynamics of premixed flames. Journal of Fluid Mechanics 116: 251-282.
12. Culick FEC (1968) A review of calculations for unsteady burning of a solid propellant. AIAA Journal 6: 2241-2255.
13. Culick FEC (2002) Combustion instabilities in solid propellant rocket motors. AIAA Paper 3592.
14. De Luca LT, Price EW, Summerfield M (1992) Nonsteady Burning and Combustion Stability of Solid Propellants. AIAA https://arc.aiaa.org/doi/book/10.2514/4.866159.
15. Flandro GA (1995) Effects of vorticity on rocket combustion stability. Journal of Propulsion and Power 11: 607-625.
16. King MK (1982) Analytical models of solid propellant combustion response. In K.K. Kuo and M. Summerfield (eds.), Fundamentals of Solid-Propellant Combustion. AIAA.
17. Klinger D (2023) Prediction of solid propellant burning rate characteristics using data-driven modelling approaches. Propellants, Explosives, Pyrotechnics.
18. Kuo, K.K. and Summerfield, M. (eds.) (1984). Fundamentals of Solid-Propellant Combustion. AIAA.
19. Law CK (2010) Combustion Physics. Cambridge University Press https://www.cambridge.org/core/books/combustion-physics/8259DA7A712262E03DD72C365F89F32E.
20. Liu J, Yinghong Wang, Xinyang Li, Junhao Cong (2023) Using the impulse method to determine high-pressure burning rates of solid propellants. Aerospace 10: 818.
21. Matalon M, Matkowsky BJ (1982) Flames as gasdynamic discontinuities. Journal of Fluid Mechanics 124: 239-259.
22. Pang W (2023) Burning rate prediction of solid rocket propellant based on machine learning and data analysis. Crystal 13: 237.
23. Ren Y (2026) A study on the integrated burning rate prediction method using machine learning and knowledge extraction. Aerospace 13: 546.
24. Sawant DA (2025) Prediction of burn rate of ammonium perchlorate-hydroxyl terminated polybutadiene solid propellant using machine learning. Aerospace Systems 8 305-316.
25. Sutton GP, Biblarz O (2017) Rocket Propulsion Elements, 9th ed. Wiley. https://ftp.idu.ac.id/wp-content/uploads/ebook/tdg/DESIGN%20SISTEM%20DAYA%20GERAK/Rocket%20Propulsion%20Elements.pdf.
26. Ustun CE, R de Freitas, E Okafor, Mahdi Shahbakhti, Xi Jiang, et al. (2025) Machine learning applications for predicting fuel ignition and flame properties: current status and perspectives. Combustion and Flame https://www.semanticscholar.org/paper/Machine-Learning-Applications-for-Predicting-Fuel-%C3%9Cst%C3%BCn-Freitas/b00321f9ca52dc7d10a9c20450ab11e0f373f0a9.
27. Williams FA (1985) Combustion Theory, 2nd ed. Benjamin/Cummings 22.
28. Xu G, Bing Wang, Bingning Jin, Zhuopu Wang, Peijin Liu, et al. (2024) Numerical study of triggered thermoacoustic instability driven by linear and nonlinear combustion response in a solid rocket motor. Physics of Fluids 36: 034110.
29. Zhang Y (2025) Numerical simulation of the gas flow of combustion products in a solid rocket motor under ignition-transient conditions. Aerospace 12: 153.
30. Zeldovich YB, Barenblatt, GI, Librovich VB, Makhviladze GM (1985). The Mathematical Theory of Combustion and Explosions. Consultants Bureau https://www.osti.gov/biblio/6082197.